Acta Crystallographica Section A
Foundations of Crystallography
ISSN 0108-7673

Received 11 August 2001
Accepted 18 October 2001

One-dimensional scattering in K-hollandite: theory and experiment

L. A. Brussaard,[a]* H. Boysen,[b] A. Fasolino[a] and T. Janssen[a]

[a]Institute of Theoretical Physics, University of Nijmegen, Postbus 9010, 6500 GL Nijmegen, The Netherlands, and [b]Institut für Kristallographie der LMU, Theresienstrasse 41, 80333 München, Germany. Correspondence e-mail: lindab@sci.kun.nl

This work comprises calculations using the Frenkel–Kontorova and double-chain models, which led to new results explaining the experimental diffraction pattern of K-hollandite. The use of a deformable host chain and a Lennard-Jones-like interchain interaction gives the best results. From these calculations, it can also be concluded that the guest as well as the host are deformed and that the system is pinned. The inclusion of Debye–Waller factors as fitting parameters is also discussed, with the conclusion they should not be used in the case of the double-chain model.

1. Introduction

Hollandite structures are of interest, both experimentally and theoretically, because they form incommensurate inclusion compounds (van Smaalen, 1994), containing two different sublattices with competing lengths in one crystallographic direction. These structures are also interesting owing to their ionic conductivity by cations.

Hollandite structures form one-dimensional parallel tunnels in which different cations can be embedded. This article concentrates on the K-hollandite $K_{1.54}Mg_{0.77}Ti_{7.23}O_{16}$ (Weber & Schulz, 1986). It contains an octahedral (Ti, Mg)-oxide framework (the host structure) forming separate channels in which the potassium ions (the guests) reside. Fig. 1 shows a sketch of the structure projected on the **ab** plane. Not all available crystallographic sites in the tunnels are occupied by potassium ions, in fact in the present case the fractional occupancy of these sites is 77%. The periodicity of the host is 2.97 Å and that of the guest 3.86 Å (= 2.97/0.77) along the c direction, in the other directions $a = b = 10.13$ Å.

A rotation photograph of X-ray scattering in K-hollandite measured by Beyeler (1976) showed the existence of diffuse layers perpendicular to $\mathbf{c}^*$. This means that the K chains in neighbouring tunnels are uncorrelated, at least to a first approximation, and, therefore, this part of the scattering can be treated in a one-dimensional way. Sections perpendicular to these layers will contain the corresponding one-dimensional Bragg peaks which are the topic of this work. A configuration model (Beyeler, 1976; Beyeler *et al.*, 1977, 1980) using a potential based on the Frenkel–Kontorova model was introduced to describe these one-dimensional experimental curves. This static model led to a Bragg scattering curve that coincides well with the experimental curve. Later work used other techniques to calculate the scattering curves, also based on the

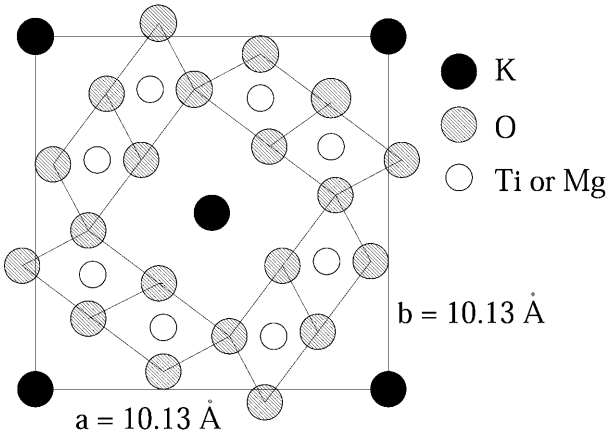

Figure 1
Structure of K-hollandite projected on the **ab** plane

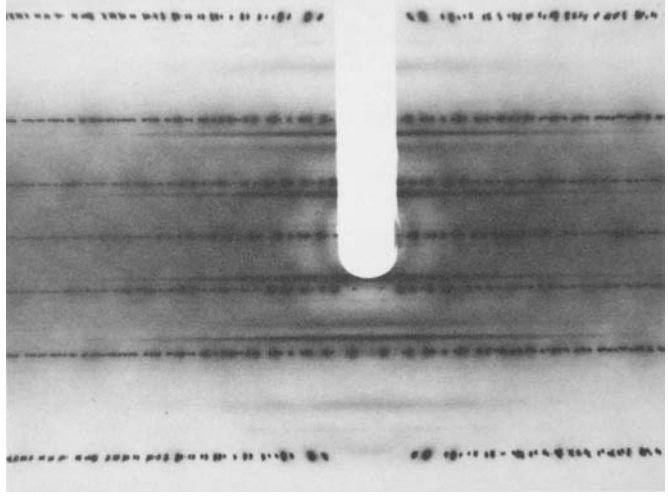

Figure 2
Oscillation photograph around the c axis (±45°) at 293 K; 6 kW rotating anode, Mo $K\alpha$ radiation; 30 h exposure time. Taken from Rosshirt (1988).

Frenkel–Kontorova model (Ishii, 1983) and one using the molecular-dynamics method (Michiue & Watanabe, 1999) based on a Coulomb interaction, Gilbert-type repulsion. These models led to the same results as were already obtained by the static configuration model.

Fig. 2 shows an X-ray rotation photograph measured by Rosshirt *et al.* (1991) that gave more information, mainly due to longer exposure times. In addition to the three layers observed by Beyeler, there are further weaker ones. A precession photograph (Rosshirt *et al.*, 1991) of the first diffuse layer of the guest structure showed the intensity distribution in this layer in more detail. The intensity distribution on the diffuse layers is not homogeneous but shows short-range-order modulations. From a detailed analysis of the symmetry of these modulation peaks and spatial considerations, it was concluded that at least part of the scattering has to be assigned also to the host structure. Because these experiments revealed much more complicated diffuse patterns, the former calculations and comparisons with the rotation photograph of Beyeler (1976) were no longer satisfactory. New calculations using a method published by Radons *et al.* (Radons *et al.*, 1985; Rosshirt, 1988; Boysen, 2001) did not lead to satisfactory results. In particular, at low wave vectors many discrepancies were found.

This article presents new calculations using the Frenkel–Kontorova and the double-chain model (Radulescu & Janssen, 1999; Brussaard *et al.*, 2001). The former model assumes that the host lattice is rigid and is represented by a sinusoidal potential, the guest is deformable and is represented by a harmonic chain of atoms. The latter gives the opportunity to study also the deformation of the host, because here both subsystems are represented by deformable harmonic chains that interact with each other. Theoretical calculations concerning the structure and Bragg spectra are presented here. The simulation of an experiment requires the incorporation of effects due to the specific experimental set-up.

The calculations use an approximation of the real incommensurate structure by introducing a large unit cell on which periodic boundary conditions are applied. The ground-state configuration and the corresponding Bragg scattering curves of the lattices are calculated. The results using the Frenkel–Kontorova system are different from the earlier results (Beyeler, 1976; Beyeler *et al.*, 1977, 1980; Ishii, 1983; Michiue & Watanabe, 1999) in showing a peak at the first main Bragg point of the host as well. The resulting scattering curves from the double-chain model coincide nicely with the experimental curve. This model shows also that not only the guest but the host structure as well is deformed. It is also shown that an interchain interaction that extends over several unit cells gives better results than a short-range interchain potential. From the modulation functions, it can be concluded that the system is pinned. The use of Debye–Waller factors for both subsystems (in the case of the double-chain model) as fitting parameters is discussed.

The article is organized as follows. §2 presents the models used to calculate the Bragg scattering curve of the guest chain in K-hollandite. §3 presents the results of the calculations. §4 discusses the results. In §5, conclusions are drawn.

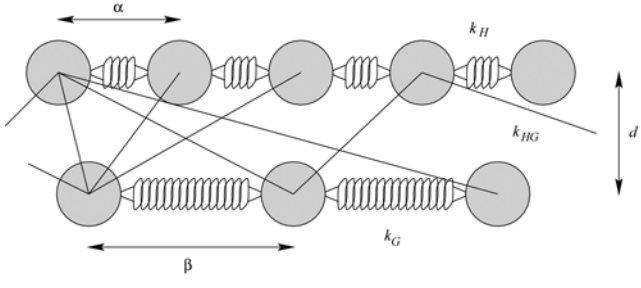

Figure 3
The double-chain model. The intrachain potentials (indicated by springs) are harmonic. The interchain potential is either Lennard-Jones like or Gaussian. The distance d between the chains is fixed. The equilibrium distances between particles in the chains are α and β, respectively.

2. Models

This work uses two related models. The first is the Frenkel–Kontorova model (Frenkel & Kontorova, 1938), which consists of a harmonic chain (V_G) on a rigid sinusoidal potential (V_H). The potential energy of this model can be written as

$$V = V_G + V_H = \frac{k_G}{2}\sum_i (x_i - x_{i-1} - \beta)^2 - \frac{V_o}{2}\sum_i \cos\left(\frac{2\pi}{\alpha}x_i\right), \quad (1)$$

where k_G is the force constant of the chain, β is the periodicity of the chain, x_i are the positions of the atoms in the chain, V_o is the strength of the substrate potential and α is the periodicity of this potential. The first term describes the guest chain, the second term represents the potential due to the host structure.

The second model is an extension of the previous model: the double-chain model (Radulescu & Janssen, 1999; Brussaard *et al.*, 2001), where the substrate potential is replaced by a second deformable chain. Fig. 3 shows a sketch of this model. In this article, the upper chain corresponds to the host structure and the lower chain to the guest structure in K-hollandite. The potential energy for this model can be written as follows:

$$V = V_H + V_G + V_{HG} = \frac{k_H}{2}\sum_i (x_i - x_{i-1} - \alpha)^2 + \frac{k_G}{2}\sum_j (y_j - y_{j-1} - \beta)^2 + k_{HG}\sum_i\sum_j \Phi(x_i - y_j), \quad (2)$$

where k_H and k_G are the force constants of the host and guest intrachain potentials, α and β the equilibrium distances, x_i and y_j the positions of the ith and jth particles of the first and second chains, respectively, and k_{HG} is the strength of the interchain potential $\Phi(r)$.

This article uses two different interchain potentials, the first being a Gaussian potential which is written as

$$\Phi(x_i - y_j) = -\frac{1}{2}\rho^2 \exp\left[-\left(\frac{x_i - y_j}{\rho}\right)^2\right], \qquad (3)$$

where ρ denotes the width of the potential well. At a distance of 9 Å, which is much larger than ρ, the Gaussian potential was cut off. The other interchain potential used is a Lennard-Jones-like potential:

$$\Phi(r) = \left[\left(\frac{r^2 + d^2}{\sigma^2}\right)^{-6} - \left(\frac{r^2 + d^2}{\sigma^2}\right)^{-3}\right], \qquad (4)$$

where d is the fixed distance between the two chains and σ denotes where the potential crosses the zero axis. The parameters σ and d equal 1 and 1.2 Å, respectively, in the numerical calculations. The minimum of the Lennard-Jones potential is at a smaller distance ($r = 1.12$ Å) than the distance d, so that only the attractive part beyond the minimum of the Lennard-Jones potential plays a role. The potential is cut off at a distance of about 570 Å using a cut-off function to avoid singularities in the derivatives that are used in the minimization of the potential energy (2).

In both models, the masses of the particles are taken as unity. The models are one-dimensional and the particles are allowed to move only in the chain direction. A large unit cell was chosen in the numerical calculations as an approximation to the real incommensurate crystal. The periodicity of the host is in both models $\alpha = 2.97$ Å, in the case of the double-chain model there are 55 particles in the host chain. In both models, the guest chain contains 42 particles and has a periodicity $\beta = 3.89$ Å to match the required ratio in the real crystal as closely as possible. On this large unit cell, periodic boundary conditions are applied.

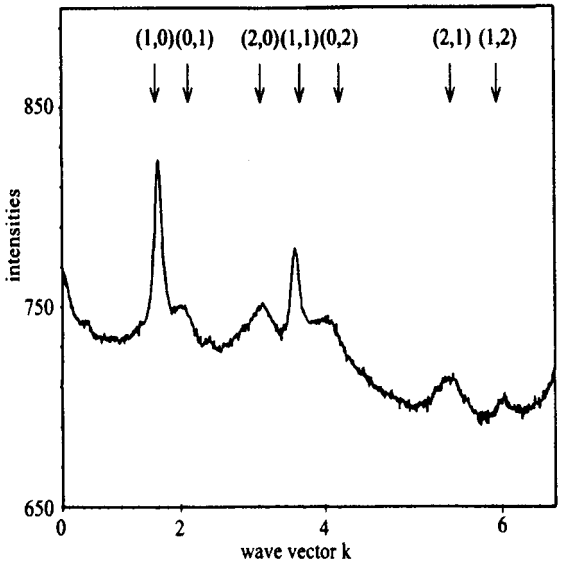

Figure 4
The intensities of the experimental scattering on a line normal to the diffuse sheets. The line is chosen so that the main Bragg peaks of the host are avoided.

The steps followed in the numerical calculations are as follows. First the equilibrium positions of the particles are found by minimizing the potential energies (1) or (2). This was performed numerically using a quasi-Newton [the Broyden–Fletcher–Goldfarb–Shanno algorithm (Press *et al.*, 1996)] method. The system parameters, *i.e.* the lattice periodicities, the force constants and the parameters of the interchain potentials, were kept fixed during the minimization procedure. The equilibrium configuration of the chain in the absence of the substrate potential was used as a starting point for the minimization routine in the first model. In the second model, the input configuration is formed by the equilibrium positions of the particles in the absence of the interchain potential. From the minimum configuration, the modulation functions can be calculated (Brussaard *et al.*, 2001).

Next, the one-dimensional Bragg scattering curve is calculated. The intensity distribution $S(k)$ is proportional to the square of the geometrical structure factor $G(k)$:

$$S(k) \propto |G(k)|^2 = \sum_i^n \sum_j^n \exp[ik(z_i - z_j)], \qquad (5)$$

where k is the difference between the incoming and outgoing wave vectors and z stands for x or y, the positions of the particles in the chains after minimization. For comparison with experimental results, this calculated Bragg scattering curve can be modified by instrumental factors like the Lorentz or polarization factor, for a discussion on these see §4. If only the positions of the guest chain are taken into account (in the case of the double-chain model), one obtains the scattering curve of the guest structure. The curve found using this equation was smoothed using a moving Hann window (Press *et al.*, 1996).

For the double-chain model, the scattering curve of the total system contains Bragg peaks due to the host and to the guest structures. The former are at wave vectors $2n\pi/\alpha$ and the latter at $2m\pi/\beta$, where n and m are integers. Beside these main peaks, there will also be satellite reflections at wave vectors $2n\pi/\alpha + 2m\pi/\beta$ with both n and m nonzero. The labelling of these peaks will be (m, n), where m stands for contributions from the guest and n from the host lattice. Note that the main peaks of the host $(0, n)$ contain also contributions from the guest and *vice versa* owing to the mutual modulation, *i.e.* the modulation function of the host has the period of the guest structure and *vice versa*. In order to obtain the one-dimensional part of interest here, which is due to the guest structure only, the scattering from the unperturbed host structure is subtracted from the scattering from the total system in one of the performed model calculations. Note that in the notation used here the first index refers to the guest, the second to the host, for compatibility with previous work.

3. Results

Fig. 2 shows the oscillation photograph (Rosshirt, 1988; Rosshirt *et al.*, 1991) of K-hollandite around the c axis measured by E. Rosshirt. Along a line perpendicular to the layers, the gray scale can be converted into intensities (without using integrated intensities) as was performed in Rosshirt

(1988). Fig. 4 shows the results (Rosshirt, 1988) for such a line. Other parallel lines show similar intensity distributions. The selected line was chosen so that the main three-dimensional Bragg reflections of the host structure were avoided. Indicated in the figure are main Bragg reflections of the guest and satellite reflections. To the right of the peaks at $(1, 0)$ and $(1, 1)$, the weaker peaks (or shoulders) visible in the figure can be labelled $(0, 1)$ and $(0, 2)$. Note that these peaks are missing in the curves presented by Beyeler (1976).

For the Frenkel–Kontorova model, the best results were obtained by choosing k_G and V_o equal to 0.19 and 0.24, respectively. Fig. 5 shows the resulting scattering curve. Contrary to former calculations (Beyeler *et al.*, 1980; Ishii, 1983; Michiue & Watanabe, 1999), there is a peak at $(0, 1)$. At $(0, 2)$ no peak is found and an extra but weak broad peak is found at $(3, \bar{1})$.

In the double-chain model, first the Gaussian potential (3) was chosen as the interchain potential Φ. Fig. 6 shows two different resulting scattering curves. Note that the system parameters are different in the two cases. Curves that agree best with the experiment are shown. The curve resulting from a somewhat wider potential well (solid line in the figure) agrees better with the experimental curve than in case of the narrower well, *i.e.* smaller value for the parameter ρ. However, both curves do not give a satisfactory agreement with the experimental Bragg scattering curve. In the case of the larger ρ, peaks are found in the same places as in the experiment, except the last one, $(1, 2)$, which is missing in the numerical calculation. There is an additional one at $(3, 0)$, which is not present in the experiment. From the curve for smaller ρ, it can be concluded that this does not correspond at all to the experimentally found curve. The force constants for this curve are rather unrealistic but these gave the best resulting curve.

The Lennard-Jones-like potential (4) has a longer range than the Gaussian potential. Fig. 7 shows the results for these calculations. The choice made for the values of the force constants is $k_H = 25$, $k_G = 1.1$ and $k_{HG} = 2.98$, which gave the best results compared with the experimental scattering curve. There are three curves in Fig. 7, corresponding to the same choice of system parameters. The solid line gives the scattering from all particles in the unit cell, guest as well as host systems. The dashed line gives the scattering curve when only the guest structure is considered, the dotted line when only the host structure is taken into account.

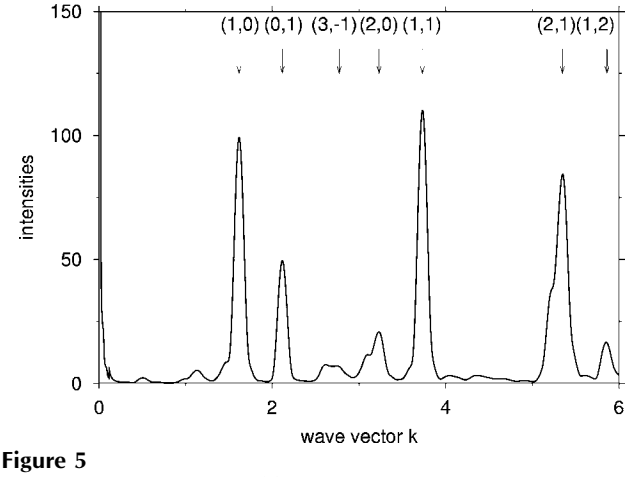

Figure 5
Bragg scattering curve $S(k)$ using the Frenkel–Kontorova model. Indicated are the indices of the Bragg peaks with appreciable intensity. The system parameters are: $\alpha = 2.97$, $\beta = 3.89$ Å, $k_G = 0.19$ and $V_o = 0.24$ and 42 particles in the guest chain.

4. Discussion

In this section, first the calculated scattering curves are compared to the experimental curves and the differences are discussed. Then the found ground states and modulation

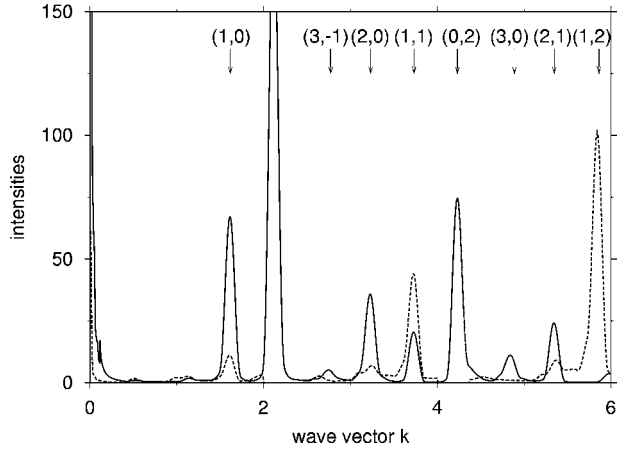

Figure 6
The scattering curves $S(k)$ using the double-chain model and a Gaussian interchain potential for two choices of system parameters. The values of the system parameters for the solid line are: $\alpha = 2.97$, $\beta = 3.89$ Å, $\rho = 0.95$, $k_H = 25$, $k_G = 1.1$ and $k_{HG} = 2.0$. Dashed line: $\alpha = 2.97$, $\beta = 3.89$ Å, $\rho = 0.33$, $k_H = 10000$, $k_G = 0.1$ and $k_{HG} = 2.5$. In both cases, there are 55 particles in the host and 42 particles in the guest chain.

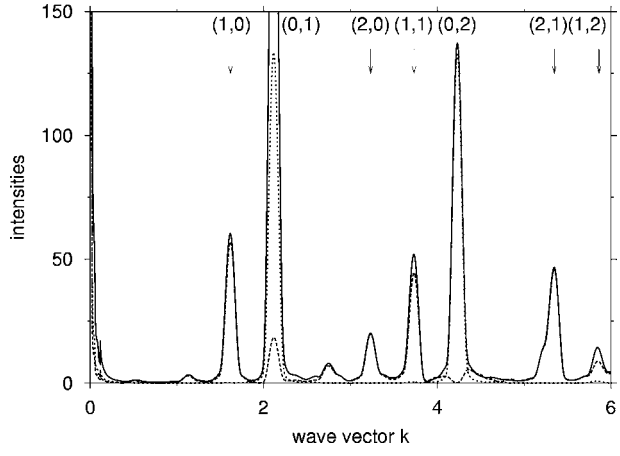

Figure 7
Scattering curves $S(k)$ obtained using the double-chain model with Lennard-Jones interchain interaction. The system parameters are: $\alpha = 2.97$, $\beta = 3.89$ Å, $k_H = 25$, $k_G = 1.1$ and $k_{HG} = 2.98$. There are 55 particles in the host and 42 particles in the guest chain. The solid line corresponds to the scattering from the total system, the dashed line to scattering from the guest structure and the dotted line to scattering from the host structure.

functions are discussed. Thirdly, the broadening of some peaks is considered, followed by a discussion about factors (treated is the Debye–Waller factor) that can improve the calculated results. Finally, the comparisons between the calculated and measured curves are made quantitative.

The calculations shown in Figs. 5 and 7 show also a peak at $(0, 1)$ as a result of the scattering at the guest chain. This peak was not found in the former experimental measurements (Beyeler, 1976) and the corresponding calculations (Beyeler *et al.*, 1980; Ishii, 1983; Michiue & Watanabe, 1999). However, at least a weak contribution to this peak from the guest can be expected, as the guest has a modulation function with periodicity equal to that of the host structure, as mentioned in §2. This explains the shoulder found in the experiment shown in Fig. 4 at this peak. However, in this experimental curve a shoulder with index $(0, 2)$ is also visible, while in the calculations an extinction was found in both models. This could mean that the selected line perpendicular to the diffuse layers still cuts the edges of the main Bragg spots of the host. The details of the former calculations are not known, but it is possible that here the contribution to the scattering at $(0, 1)$ and $(0, 2)$ is suppressed in some way.

The scattering curve due to the host in Fig. 7 shows very weak contributions to satellite peaks $(1, 1)$ and $(1, 2)$, indicating that the host is modulated. The modulation function of the host (see Fig. 8) shows more clearly the deformation, though the displacements of the host molecules are a factor of 10 smaller than those of the potassium ions. From the fact that the modulation functions are discontinuous, it can be concluded that the system is pinned so that the potassium ions cannot move freely and do not form a liquid inside the hollandite. The calculations by Radons *et al.* (1985) and Rosshirt (1988) assumed the guest chains to be liquid like and this presumably causes the bad agreement with the experiment. The pinning can also explain the activation energy of the conduction (Beyeler *et al.*, 1980) of K-hollandite, although defects in the crystal could also be partially responsible for this feature.

Fig. 9 shows a section of the ground states of both the Frenkel–Kontorova (plus) and the double-chain model (cross). The guest chain of the double-chain model (the middle chain in the figure) forms domains of mostly three ions. This is slightly different from the results found by Beyeler *et al.* (1980), where the domains contained mainly three or four ions. The guest chain of the Frenkel–Kontorova model also contains domains of three and four atoms. The differences in the ground states of the double-chain and Frenkel–Kontorova models are small (as is also visible in Fig. 8). The host lattice being rigid or deformable leads to the differences found. That the differences are small is to be expected from the fact that the Bragg scattering curves of these models are also quite similar. Note that there is a difference in approach in our calculations and those of Beyeler *et al.* The latter takes vacancies into account in the potassium chains, whereas the calculations presented here start with two periodic undisturbed chains.

In the experimental curve, the $(2, m)$ peaks are generally broader than the $(1, m)$ peaks. Extrapolating this observation, the $(3, m)$ peaks are expected to be even broader and this may be the reason that the $(3, 0)$ peak was not observed and covered in the background. Note, however, that, in the calculations using the double-chain model shown in Fig. 7, the $(3, 0)$ peak is also absent. In the calculations, the broadening of the $(2, m)$ peaks is not there. A probable cause for this lack of broadening is the use of periodic boundary conditions, which seems to lead to a coherency between the clusters (see Fig. 9) formed in the guest chain. Nevertheless, disregarding this effect, the areas underneath the peaks should be calculated correctly and only these are therefore compared in the following. Moreover, only the pure elastic Bragg scattering is calculated, while in experiment there are still inelastic contributions, which will broaden peaks with higher indices. Finally, the calculated curves resulting from (5) are smoothened, all with the same width.

As already stated, instrumental factors are not taken into account during the numerical calculations. These are factors such as polarization or absorption. If they are introduced by hand in a calculation, these factors introduce extra parameters that can be used to tune the calculated curves. For instance, the calculations can be improved by introducing Debye–Waller (DW) factors for both chains:

$$F_{\rm DW} = \exp(-2Uk^2), \tag{6}$$

where U is the square of the average displacement for a certain temperature and k the difference between the

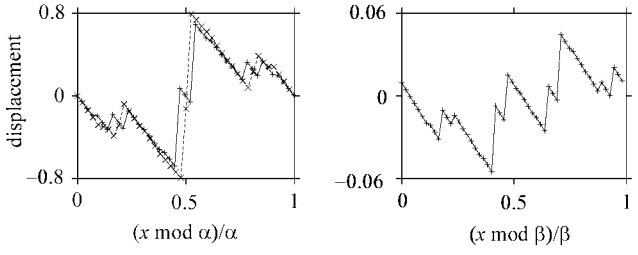

Figure 8
The modulation functions for the same system parameters as in Fig. 7 in the case of the double-chain model and in Fig. 5 in the case of the Frenkel–Kontorova model. Left: the guest chain of the double-chain model (plus) and the Frenkel–Kontorova model (cross). Right: the host chain of the double-chain model. In the case of the Frenkel–Kontorova model, the host is rigid and its modulation function is zero. The lines are a guide for the eye.

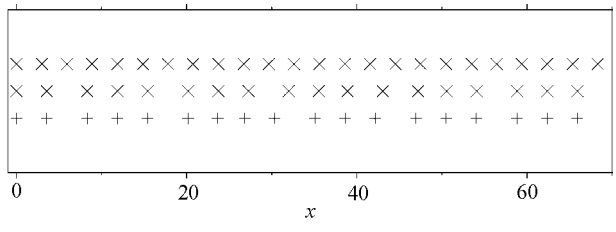

Figure 9
Part of the ground states of the Frenkel–Kontorova model (plus) and the double-chain model (cross) for the same system parameters as in Fig. 5 and Fig. 7, respectively. The upper chain is the host chain and the middle chain the guest chain of the double-chain system.

Table 1
The difference of the calculated peaks with experiment (for details see text).

The first five columns are calculations performed with the double-chain model with the system parameters as in Fig. 7, the last with the Frenkel–Kontorova system with parameters as in Fig. 5. The first column corresponds to the scattering of the total system, the second of the guest, the third of the total system minus the host in equilibrium, the fourth of the total system minus the host in equilibrium when DW factors are taken into account, the fifth of the guest with DW factors included and the last is just at the chain in the Frenkel–Kontorova model. The last line gives the sum of the squared numbers in the corresponding columns, denoted by *R*.

(n, m)	1	2	3	4	5	6
(1, 0)	−0.20	−0.05	−0.15	−0.09	0.07	−0.09
(0, 1)	0.44	−0.03	0.26	0.34	0.0	0.0
(2, 0)	−0.14	−0.08	−0.12	−0.12	−0.07	−0.12
(1, 1)	−0.05	0.07	0.01	−0.02	0.05	0.11
(2, 1)	−0.03	0.09	0.01	−0.07	−0.01	0.11
(1, 2)	−0.02	0.01	−0.01	−0.03	−0.03	0.0
R	0.26	0.02	0.10	0.14	0.01	0.05

incoming and outgoing wave vectors. For the host and guest structures, different values for U can be chosen. Fig. 10 shows the results including this effect. The solid curve shows the Bragg scattering curve of the total system minus the Bragg scattering that would come from the unperturbed host chain. The dashed curve is the same but here the DW factors were introduced in the calculations. It was assumed that the potassium ions are lighter and therefore more mobile than the atoms in the host structure. In this case, the chosen values for U were 0.01 Å^2 for the host and 0.02 Å^2 for the guest chain. In this way, the peak at (2, 1) is suppressed more than its direct neighbour at (1, 2) and the results are a little closer to the experimental curve.

The great impact of the use of DW factors in describing temperature effects is shown in Fig. 11. This figure shows the Bragg scattering curve of the guest chain for the following choice of force constants: $k_H = 10$, $k_G = 1.8$ and $k_{HG} = 3.5$. The value for U was 0.07 Å^2 for the guest ions. The curve without the DW factor (solid line) still shows peaks at high wave vectors. However, with the DW factor (dashed line) they are almost gone, which is also the case for the experimentally found curve in Rosshirt (1988) measured at high temperature (875 K). The results are better if the scattering curve from the total system minus the scattering of the equilibrium state of the host is considered, taking a DW factor of 0.04 Å^2 for the host structure.

However, the use of the DW factor as a fitting parameter is not preferable. Whether the chosen DW factors are correct is not a trivial question. The initial equation (2) does not depend explicitly on temperature. The DW factors are included by hand and the values for U were chosen such that the resulting curve agrees best with the experimental curve. Therefore it is not clear whether these found values correspond indeed to the thermal displacement at the experimentally used temperature (in this case room temperature or 875 K).

The contribution of instrumental factors (Lorentz, polarization factors) was estimated and showed that the combination of all these factors can be fitted to a reasonable approximation by a pseudo DW factor within the actual range of the measurements with an overall 'instrumental' mean square displacement of $U \approx 0.034$ Å^2. The form factor of the guest (potassium) has been assumed to apply also for the host, because, without thorough three-dimensional calculations, it is difficult to estimate to what extent the number of O atoms and other cations has to be taken into account. Since, however, the contribution of the host is small, this further simplification can be tolerated as a first approximation.

The inclusion of two extra parameters, the DW factor for the host and the guest, respectively, only decreases the value of R (Table 1, see last paragraph for more details) by a factor 2. The effect is not as big as expected and apparently the results without the DW factors already give a good description

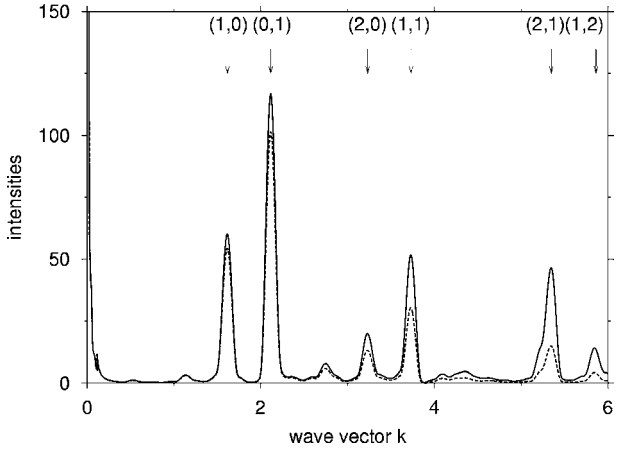

Figure 10
Scattering curves $S(k)$ using the double-chain model for the same system parameters as in Fig. 7. The solid line shows the scattering curve of the undistorted host chain subtracted from the total scattering curve of the system after minimization. The dashed line corresponds to the same calculation, but with DW factors incorporated.

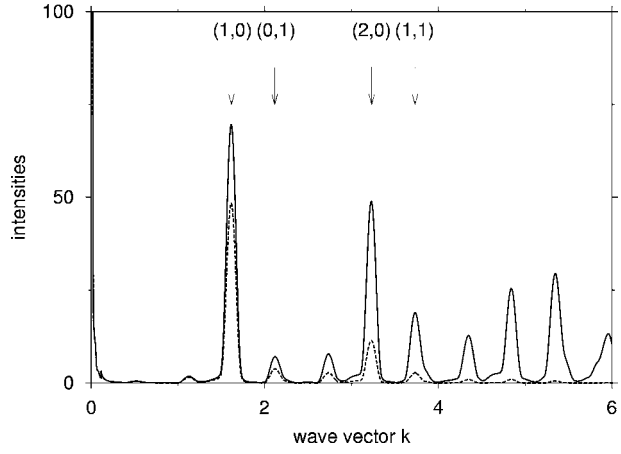

Figure 11
Scattering curves $S(k)$ of the guest chain using the double-chain model. The solid line is without and the dashed line with a DW factor. The latter agrees nicely with the high-temperature (875 K) measurement of Rosshirt (1988). The system parameters are the same as in Fig. 7 except $k_H = 10$, $k_G = 1.8$ and $k_{HG} = 3.5$

of the real system. In the case of the calculation at high temperature, the effect is larger, though the discrepancies from the experimental curve are also larger than at room temperature.

The modulation of the host due to the interaction with the guest shows displacements from its equilibrium positions between −0.06 and 0.05 Å for room temperature, −0.12 and 0.11 Å for high temperature, while the average displacement due to the included DW factor is 0.1 Å ($0.01^{1/2}$) and 0.2 Å ($0.04^{1/2}$), respectively. This means that the thermal displacement is almost twice as large as the static displacement due to the competing forces in the double-chain system. When the thermal displacement is added to the modulation function, the non-analyticity is not clear any more. So it is no longer evident that the host subsystem is also pinned. Therefore, the validity of the double-chain model using DW factors becomes doubtful. The system at high temperature is, owing to the great influence of the DW factors, not as sensitive to a change in force constants as it is at room temperature.

The DW factors can be calculated using the phonon spectrum and the Bose distribution to find the occupied phonons at a certain temperature. This eventually leads to the average thermal displacement of the molecules in the subsystems. This dynamic calculation is out of the scope of this article. The other way around is also possible, to find the temperature belonging to a certain value of U, but this is also not a trivial procedure. Another difficulty is the fact that the DW factors involve three-dimensional dynamics whereas the model is one-dimensional.

The comparisons between the experimental and calculated curves made so far are not yet quantitative. There are many ways to quantify the results and here a rather simple but effective method is chosen. The area below a peak was calculated and this number was divided by the area under all the peaks taken into account. The peak at $(0, 2)$ was not considered as it is not found in all the calculations and its origin in the experiment is not clear. The last step of the calculation was to subtract the experimentally found areas from the calculated ones. Table 1 shows the results. From these numbers, it can be deduced that the scattering curve of the guest using DW factors (fifth column) gives the best agreement. Here the smallest numbers are found as is shown in the bottom row of the table, where the squares of the numbers in each column are summed. Note that in the Frenkel–Kontorova model the scattering takes place only at the guest chain. The results for the Frenkel–Kontorova model turn out to be the third best match with the experimentally found curve. The second best is the scattering at the guest chain in the double-chain model, given in the second column. But the introduction of two extra fitting parameters by taking into account the pseudo DW factors (fifth column) does not dramatically improve the calculations compared with the results in the second column, which already describe well the experimental curve. This also means that the experimentally found curve in Fig. 4 shows indeed the Bragg scattering of the guest and that the modulation of the host is of importance for the resulting scattering curve.

5. Conclusions

The experiments (Rosshirt, 1988; Rosshirt *et al.*, 1991) measuring the one-dimensional Bragg scattering of K-hollandite showed more complicated patterns than earlier measurements and calculations (Beyeler, 1976; Beyeler *et al.*, 1977, 1980; Ishii, 1983; Michiue & Watanabe, 1999) had shown so far. Attempts to model (Radons *et al.*, 1985; Rosshirt, 1988) the structure were made, but those results were not very satisfactory. Calculations performed in this article using the Frenkel–Kontorova and double-chain models result in scattering curves that agree very well with the experimental curve. It was found that the interaction between the two subsystems is indeed not short range.

Our calculations show a peak at $(0, 1)$, *i.e.* the main Bragg peak of the host, in the scattering of the guest chain. A weak contribution can be expected, and this explains the weak peak found in the experiment.

The double-chain model shows that the host chain is indeed deformed although, being an order of magnitude stiffer than the guest, its deformation is only weak (ten times less compared with that of the guest). Therefore, the scattering curve of the host contains primarily the main Bragg peaks, although very weak contributions to satellites were observed as well.

From the modulation functions of both the Frenkel–Kontorova model and the double-chain model, it can be concluded that the system is pinned. This means that the subsystems cannot move freely over each other. This explains the bad agreement of the calculations first performed to explain the new experiments (Radons *et al.*, 1985; Rosshirt, 1988), where it was assumed that the potassium ions form a liquid-like system in the channels. It was found that the interaction between the two subsystems is indeed not short range.

Modifying the calculated Bragg scattering curve by instrumental factors will lead to a better comparison to specific instrumental results. The introduction of pseudo DW factors showed this. However, the calculated scattering curve using (5) (the square of the geometrical structure factor) agrees very well with the experimental results. Therefore, the presented double-chain model explains the Bragg scattering at K-hollandite independent of the specific experimental set-up.

This work is supported by Stichting Fundamenteel Onderzoek der Materie with financial support of the Nederlandse Organisatie voor Wetenschappelijk Onderzoek.

References

Beyeler, H. U. (1976). *Phys. Rev. Lett.* **37**, 1557–1560.
Beyeler, H. U., Pietronero, L. & Strässler, S. (1980). *Phys. Rev. B*, **22**, 2988–3000.
Beyeler, H. U., Pietronero, L., Strässler, S. & Wiesmann, H. J. (1977). *Phys. Rev. Lett.* **38**, 1532–1535.
Boysen, H. (2001). *Ferroelectrics*, **205**, 7–12.
Brussaard, L. A., Fasolino, A. & Janssen, T. (2001). *Phys. Rev. B*, **63**, 214302-1–214302-7.
Frenkel, J. & Kontorova, T. (1938). *Phys. Z. Sowjetunion*, **13**, 1.

Ishii, T. (1983). *J. Phys. Soc. Jpn*, **52**, 4066–4073.
Michiue, Y. & Watanabe, M. (1999). *Phys. Rev. B*, **59**, 11298–11302.
Press, W. H., Teukolsky, S. A., Vettering, W. T. & Flannery, B. P. (1996). *Numerical Recipes in C, the Art of Scientific Computing*, 2nd ed. Cambridge University Press.
Radons, G., Keller, J. & Geisel, T. (1985). *Z. Phys.* B**61**, 339–352.
Radulescu, O. & Janssen, T. (1999). *Phys. Rev. B*, **60** 12737–12745.
Rosshirt, E. (1988). Thesis, Universität München, Germany.
Rosshirt, E., Frey, F. & Boysen, H. (1991). *Neues Jahrb. Mineral. Abh.* **163**, 101–115.
Smaalen, S. van (1994). *Crystallogr. Rev.* **4**, 79–202.
Weber, H. P. & Schulz, H. (1986). *J. Chem. Phys*, **85**, 475–484.